Journal of Molecular Structure 1081 (2015) 381–388

Contents lists available at ScienceDirect

Journal of Molecular Structure

journal homepage: www.elsevier.com/locate/molstruc

A joint experimental and theoretical study on the electronic structure and photoluminescence properties of $Al_2(WO_4)_3$ powders

F.M.C. Batista [a], F.A. La Porta [b,c], L. Gracia [b,c], E. Cerdeiras [a], L. Mestres [a], M. Siu Li [d], N.C. Batista [e], J. Andrés [b], E. Longo [c], L.S. Cavalcante [e,*]

[a] Departament de Química Inorgànica, Facultat de Química, Universitat de Barcelona, 08028 Barcelona, Spain
[b] Departament de Química Física i Analítica, UJI – Universitat Jaume I, Av. de Vicent Sos Baynat, s/n, Castelló de la Plana, 12071, Spain
[c] Universidade Estadual Paulista, P.O. Box 355, 14801-907 Araraquara, SP, Brazil
[d] IFSC-Universidade de São Paulo, P.O. Box 369, 13560-970 São Carlos, SP, Brazil
[e] CCN-DQ-GERATEC, Universidade Estadual do Piauí, João Cabral, N. 2231, P.O. Box 381, CEP: 64002-150 Teresina, PI, Brazil

HIGHLIGHTS

- $Al_2(WO_4)_3$ powders were obtained by the coprecipitation/calcination methods.
- Rietveld refinement data were employed to $[AlO_6]/[WO_4]$ clusters modeling.
- Electronic structure of $Al_2(WO_4)_3$ was performed by the density functional theory.
- A correlation between the theoretical and experimental optical band gap was observed.
- Singlet excited state is very important to photoluminescence properties of $Al_2(WO_4)_3$.

GRAPHICAL ABSTRACT

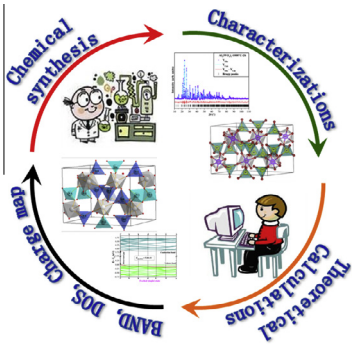

ARTICLE INFO

Article history:
Received 22 July 2014
Received in revised form 7 October 2014
Accepted 9 October 2014
Available online 27 October 2014

Keywords:
$Al_2(WO_4)_3$
Electronic structure
Clusters
DFT calculations
Photoluminescence

ABSTRACT

In this paper, aluminum tungstate $Al_2(WO_4)_3$ powders were synthesized using the co-precipitation method at room temperature and then submitted to heat treatment processes at different temperatures (100, 200, 400, 800, and 1000 °C) for 2 h. The structure and morphology of the powders were characterized by means of X-ray diffraction (XRD), Rietveld refinement data, and field emission scanning electron microscopy (FE-SEM) images. Their optical properties were examined with ultraviolet–visible (UV–vis) diffuse reflectance spectroscopy and photoluminescence (PL) measurements. XRD patterns and Rietveld refinement data showed that $Al_2(WO_4)_3$ powders heat treated at 1000 °C for 2 h have a orthorhombic structure with a space group (*Pnca*) without the presence of deleterious phases. FE-SEM images revealed that these powders are formed by the aggregation of several nanoparticles leading to the growth of microparticles with irregular morphologies and an agglomerated nature. UV–vis spectra indicated that optical band gap energy increased from 3.16 to 3.48 eV) as the processing temperature rose, which was in turn associated with a reduction in intermediary energy levels. First-principle calculations were

* Corresponding author. Tel.: +55 86 3351 8111, mobile: +55 86 9808 4129.
E-mail address: laeciosc@bol.com.br (L.S. Cavalcante).

http://dx.doi.org/10.1016/j.molstruc.2014.10.016
0022-2860/

performed in order to understand the behavior of the PL properties using density functional theory at the B3LYP calculation level on periodic model systems and indicate the presence of stable electronic excited states (singlet). The analyses of the band structures and density of states at both ground and first excited electronic states provide insight into the main features, based on structural and electronic order–disorder effects in octahedral [AlO_6] clusters and tetrahedral [WO_4] clusters, as constituent building units of this material.

Introduction

Aluminum tungstate $Al_2(WO_4)_3$ is an important semiconductor material belonging to the family of trivalent tungstates compounds with general formula $X_2(WO_4)_3$, where [X = Y^{3+}, Sc^{3+}, In^{3+}, Al^{3+} and rare earths as lanthanides (Ho–Lu)]. This oxide has attracted wide interest of several researchers due to excellent physical and chemical properties [1–9]. Moreover, $Al_2(WO_4)_3$ has an orthorhombic structure with *Pnca* space group [10,11], in which a larger pore framework structure formed by octahedral [AlO_6] clusters and tetrahedral [WO_4] clusters can be sensed. These building blocks can be considered the constituent clusters of this system, and they are connected in such a manner that they form a layered structure with a large tunnel size, in which the Al^{3+} cations are sufficiently mobile.

In recent years, different synthetic methods have been used to obtain $Al_2(WO_4)_3$ crystals, such as co-precipitation (CP) [12,13], sol–gel [14], modified Pechini [15], solid state reaction [16], and Czochralski process [17]. In addition, metal doping processes (Eu^{3+}, Cr^{3+}, Yb^{3+}, etc.) on this material generate excellent waveguides for spectroscopy [16], luminescence properties [18], and broad band laser [19]. These doping processes provoke a change in the lattice parameters as a function of both ionic charge and radius, followed by an alteration in the electronic properties due to the ionic conductivity within the orthorhombic structure [12]. In particular, negative thermal expansion (NTE) is the most commonly electronic property studied for this compound [20–25]. The NTE behavior in this material is associated to the presence of low frequency rigid modes facilitated by their open network structure with corner linking octahedral [AlO_6] and tetrahedral [WO_4] clusters [6,24]. Theoretical research has revealed a close relationship between pressure induced amorphization and NTE in these tetrahedral bonded network structures [26]. Moreover, the high pressure behavior of NTE ceramic materials is currently of significant interest in the basic sciences for use as a temperature sensor [20].

In this paper, for the first time we report the synthesis, electronic structure and photoluminescence (PL) properties of $Al_2(WO_4)_3$ powders obtained by means of a two-step synthetic route based on the CP method followed by a calcination process. These powders were structurally and morphologically characterized by means of X-ray diffraction (XRD), Rietveld refinement and field emission scanning electron microscopy (FE-SEM). Optical properties were monitored by ultraviolet–visible (UV–vis) diffuse reflectance spectroscopy and PL measurements at room temperature. Clusters concept have been used by our group as a basic units of a given crystal [27–29], and in the present case, the different forms that are organized inside the $Al_2(WO_4)_3$ crystal structure, i.e. octahedral [AlO_6] clusters and tetrahedral [WO_4] clusters, play a key role on their physical and chemical properties. The subtle balance between the electronic order–disorder effects and distortions in clusters reflected in optical properties of $Al_2(WO_4)_3$ crystal have been addressed by first principles calculations by using the density functional theory (DFT) at the B3LYP calculation level in order to provide a framework for the interpretation of experimental data.

Experimental details

Synthesis of $Al_2(WO_4)_3$ powders by the CP method

$Al_2(WO_4)_3$ powders were prepared by the CP method at room temperature without surfactant in aqueous solutions. The typical $Al_2(WO_4)_3$ powder synthesis procedure is described as follows: 3×10^{-3} mols of tungstate (VI) sodium dihydrate [$Na_2WO_4{\cdot}2H_2O$] (99% purity, Panreac) and 2×10^{-3} mols of aluminum nitrate nonahydrate [$Al(NO_3)_3{\cdot}9H_2O$] (99% purity, Sigma–Aldrich) were dissolved separately in two plastic tubes (Falcon) with 50 mL of deionized water in each tube. The first solution with $6Na^+$ and $3WO_4^{2-}$ ions was transferred to a PYREX glass beaker with a capacity of 250 mL where it was constantly stirred for 2 min. The second solution with ($2Al^{3+}$ and $6NO_3^-$) ions was added to this mixture and a white suspension rapidly formed. In aqueous solutions, the fast reactions between $2Al^{3+}$ and $3WO_4^{2-}$ ions occur due to the force of the electrostatic attraction, resulting in the formation of amorphous or disordered $Al_2(WO_4)_3$ precipitates.

Calcination of amorphous $Al_2(WO_4)_3$ powders obtained by the CP method

The resulting suspensions were washed with deionized water several times to remove all Na^+ ions. The powders were then heat-treated at 100 °C, 200 °C, 400 °C, 800 °C and 1000 °C for 2 h. The chemical reactions between $2Al^{3+}/3WO_4^{2-}$ ions and solid state at different temperatures trigger a phase transformation from an amorphous state to a crystalline state, and/or produce a structural transition from disordered to ordered lattice, as shown in equation (1).

$$2Al^{3+}_{(aq)} + 3WO^{2-}_{4(aq)} \xrightarrow{25\ ^\circ C} Al_2(WO_4)_{3(s)} \xrightarrow{100,200,400\ ^\circ C} Al_2(WO_4)_{3(s)\text{disordered}} \xrightarrow{800,1000\ ^\circ C} Al_2(WO_4)_{3(s)\text{ordered}} \quad (1)$$

Finally, these white $Al_2(WO_4)_3$ powders were structurally and morphologically characterized using different techniques.

Characterizations of $Al_2(WO_4)_3$ powders

$Al_2(WO_4)_3$ powders were structurally characterized by XRD patterns using a X'Pert PRO MPD Alpha1 (PANalytical, USA) with Cu Kα radiation (λ = 1.5406 Å) in the 2θ range from 5° to 80° in the normal routine with a scanning velocity of 2°/min and from 10° to 110° with a scanning velocity of 0.5°/min of a 0.02° step in the Rietveld routine. Thermogravimetric analysis (TGA), differential thermogravimetric analysis (DTA) and differential scanning calorimetry (DSC) were performed using a SDT Q600 (TA instruments, USA) from room temperature to 1200 °C with a heating rate of 5 °C/min. The shapes and sizes of these $Al_2(WO_4)_3$ powders were observed with an Inspect F50 FE-SEM (FEI Company, USA) operated at 15 kV. UV–vis spectra were taken using a Varian spectrophotometer (model Cary 5G) in diffuse-reflectance mode. PL measurements were taken at room temperature through a Monospec 27 monochromator (Thermo Jarrel Ash, USA) coupled to an R446

photomultiplier (Hamamatsu Photonics, Japan). A krypton-ion laser (Coherent Innova 90 K; $\lambda = 350$ nm) was used as the excitation source; its maximum output power was maintained at 500 mW. The laser beam passed through an optical chopper, and its maximum power on the sample was maintained at 40 mW. All measurements were performed at room temperature.

Theoretical methods and model systems

All calculations were performed by using the DFT method with the B3LYP hybrid functional [30,31], as implemented in the CRYSTAL 09 computer code [32]. The large-core ECP basis derived by Hay and Wadt [33], the ECP68 has been chosen for W atoms, and the Al and O atoms are described with an all-electron by 9763-311(d631)G* for Al and 6-31G* for O atoms, respectively [34]. The level of accuracy for the Coulomb and exchange series was controlled by five thresholds set to (10^{-6}, 10^{-6}, 10^{-6}, 10^{-6}, and 10^{-12}). The shrinking (Monkhorst–Pack) [35] factor was set to 6, which corresponds to 80 independent k-points in the irreducible part of the Brillouin zone integration.

Based on the experimental refinement of the XRD results and Rietveld refinement data presented in this research, two periodic models were used to find the singlet ground (s) and excited singlet electronic states (s^*). These models can be useful to represent different structural and electronic order–disorder effects in the material. An excited state is obtained by imposing a low and high spin state that must promote an electron from the valence band (VB) to the conduction band (CB). However, it is important to note that the accurate calculation of excited electronic states of periodic systems still represents a challenge for quantum-chemical methods [36]. We have previously employed this method to show how structural disorder affects the band gap value; specifically, to shed light on the transitions associated with the PL emission behavior of perovskite (ABO_3) [37,38], tungstate (AWO_4) [39] and molybdate ($AMoO_4$) based materials [40]. Per unit cell, this involves imposing two electrons with the opposite or same spin, corresponding to the singlet and triplet electronic state, respectively. It also creates Frenkel excitons (holes in the VB, electrons in the CB). In this research, all attempts to find excited states with triplet multiplicity were unsuccessful. To confirm the character of local minima on potential energy surfaces, we calculated vibrational frequency to ensure the presence of only positive frequencies, which correspond to minima for both ground and excited singlet electronic states. The results were analyzed by calculating the density of states (DOS), band structure, charge density and band gap value. The XcrysDen program [41] was used for the drawing design of the band structure.

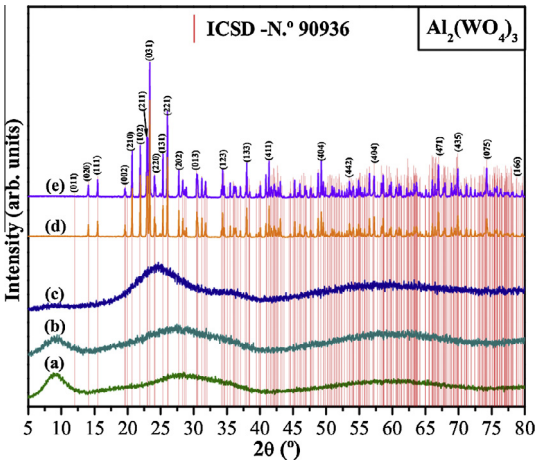

Fig. 1. (a–e) XRD patterns for the $Al_2(WO_4)_3$ powders heat-treated (a) 100 °C, (b) 200 °C, (c) 400 °C, (d) 800 °C and (e) 1000 °C for 2 h, respectively.

Results and discussion

XRD patterns analyses

Fig. 1(a–e) shows XRD patterns for $Al_2(WO_4)_3$ powders obtained using the CP method and heat-treated at different temperatures for 2 h.

An analysis of the results found that the as-synthesized powders at 100 °C, 200 °C, and 400 °C for 2 h did not exhibit diffraction peaks; therefore, they are amorphous or structurally disordered at long range (see Figs. 1(a–c)). Moreover, the decomposition process of amorphous precursor powder was complemented by TGA evolved gas analysis and DTA. The TGA and DTA curves we observed water loss at about 145 °C and our results indicate that the temperature required to crystallize $Al_2(WO_4)_3$ powders is 600 °C (see Supplementary data; Fig. S1(a and b)). In general, $Al_2(WO_4)_3$ powders heat–treated at 800 °C and 1000 °C for 2 h exhibited all diffraction peaks related to the pure phase which can be indexed perfectly to a orthorhombic structure with a space group (*Pnca*) with four molecular formula per unit cell ($Z = 4$) and a respective inorganic crystal structure database (ICSD; No. 90936) [42].

Structural representation of $Al_2(WO_4)_3$ crystals

Fig. 2 shows a schematic representation of an orthorhombic $Al_2(WO_4)_3$ unit cell modeled from the Rietveld refinement data of $Al_2(WO_4)_3$ powders heat–treated at 1000 °C for 2 h.

This unit cell illustrated in Fig. 2 was obtained by means of Rietveld refinement data to system more organized. The lattice parameters, unit cell volume, atomic coordinates and site occupation were obtained and calculated using the Rietveld refinement method [43], using the ReX Powder diffraction program version 0.7.4 [44]. Moreover, the Rietveld refinement data were used to model these unit cells using the Visualization for Electronic and Structural Analysis (VESTA) program, version 3.2.1, for Windows64bit [45]. These data are listed and illustrated in the (Supplementary data file; Table S1 and Fig. S2).

This unit cell illustrated in Fig. 2 is assigned to an orthorhombic structure of $Al_2(WO_4)_3$ crystals, which is characterized by exhibiting a space group *Pnca* and four molecular formula per unit cell ($Z = 4$) [46,47]. In these unit cells, basically the Al atoms are coordinated to six O atoms which form the distorted octahedral [AlO_6] clusters, while the W atoms are coordinated to four O atoms which form [WO_4] clusters with a tetrahedral polyhedral configuration, which are illustrated in Fig. 2.

In particular, refinement results point out that the tetrahedral [WO_4] clusters are highly distorted in the lattice and exhibit a particular characteristic related to differences in the O–W–O bond angles. There are two types of [WO_4] clusters: [$W1O_4$] and [$W2O_4$], being the latter more distorted than the former (Supplementary data Fig. S3). This result can be related to the experimental conditions required to obtain pure $Al_2(WO_4)_3$ crystals. FE-SEM images revealed large particles of crystalline $Al_2(WO_4)_3$ powders with irregular shapes (see Supplementary data; Fig. S4(a–e)). Specifically, the random aggregation process among the small particles resulted in the formation of irregular-shaped crystallites. We believe that particle growth is related to mass transport mechanisms via nanocrystalline particle diffusion during the sintering process brought about by an increase in the heat treatment. A detailed study of these mechanisms goes beyond the scope of this work, although they will be the subject of future research.

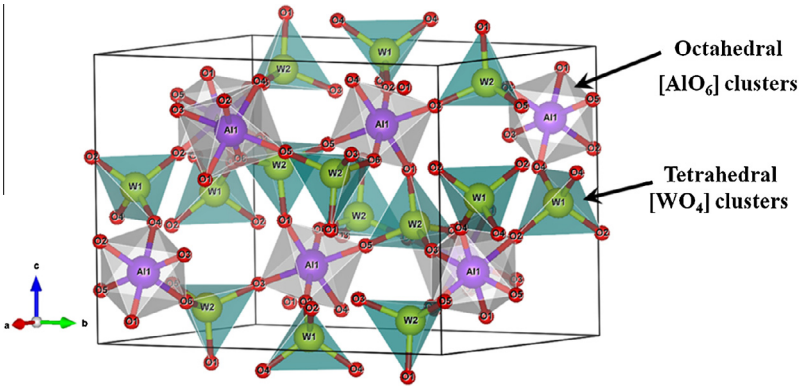

Fig. 2. Schematic representation of the orthorhombic unit cells corresponding to $Al_2(WO_4)_3$ crystals.

Table 1
Optimized lattice parameters, bond distances and angles bonds [(Al–O); (W1–O); (W2–O)] for the singlet (s) and excited singlet (s^*) electronic states.

$Al_2(WO_4)_3$ lattice	Singlet (s)	Excited singlet (s^*)
a	8.991	9.011
b	12.343	12.402
c	8.942	9.000
Al–O	1.870(1), 1.876(1), 1.888(1)	1.874(1), 1.876(1), 1.878(1)
	1.894(1), 1.911(1), 1.932(1)	1.892(1), 1.899(1), 1.936(1)
W1–O	1.726(2), 1.730(2)	1.748(2), 1.752(2)
W2–O	1.726(2), 1.731(1), 1.733(1)	1.726(1), 1.731(1), 1.734(1), 1.736(1)

Table 1 shows the values for the optimized Al–O and W–O distances and O–W–O bond angles for the ground singlet (s) and excited singlet (s^*) electronic states.

The calculated distance values between W–O of 1.726 Å are in good agreement with the experimental result of 1.794 Å. The calculated and experimental geometries (given in parentheses) for the s model, which belongs to the orthorhombic space group *Pnca*, consist of lattice parameters and unit cell volume: a = 8.991 (9.1386) Å; b = 12.343 (12.6234) Å and c = 8.942 (9.0438) Å; and V = 992.29 (1043.29)Å^3. The orthorhombic structure in s^* state expanded somewhat in the three directions of the crystal. There is an expansion of tetrahedral [W1O$_4$] clusters while a distortion of tetrahedral [W2O$_4$] more noticeable in s^* state compared to the ground state (Supplementary data Fig. S3). Based on our theoretical results, total energy variation between s^* and s states is 0.35 eV.

Electronic structure and UV–visible absorption spectroscopy analyses of $Al_2(WO_4)_3$ crystals

The optical band gap energy (E_{gap}) was calculated using the method proposed by Kubelka and Munk [48], which is based on the transformation of diffuse reflectance measurements to estimate E_{gap} values with good accuracy within the limits of assumptions when modeled in three dimensions [49]. It is particularly useful in limited cases of an infinitely thick sample layer. The Kubelka–Munk equation for any wavelength is described by Eq. (2):

$$\frac{K}{S} = \frac{(1-R_\infty)^2}{2R_\infty} \equiv F(R_\infty) \tag{2}$$

where $F(R_\infty)$ is the Kubelka–Munk function or absolute reflectance of the sample. In our case, magnesium oxide (MgO) was the standard sample in reflectance measurements. $R_\infty = R_{sample}/R_{MgO}$ (R_∞ is the reflectance when the sample is infinitely thick), k is the molar absorption coefficient and s is the scattering coefficient. In a parabolic band structure, the optical band gap and absorption coefficient of semiconductor oxides [50] can be calculated by Eq. (3):

$$\alpha h\nu = C_1(h\nu - E_{gap})^n \tag{3}$$

where α is the linear absorption coefficient of the material, $h\nu$ is the photon energy, C_1 is a proportionality constant, E_{gap} is the optical band gap and n is a constant associated with different kinds of electronic transitions (n = 0.5 for a direct allowed, n = 2 for an indirect allowed, n = 1.5 for a direct forbidden and n = 3 for an indirect forbidden). According to the literature [51–54], tungstate crystals exhibit an optical absorption spectrum governed by direct or indirect electronic transitions.

The band structure and DOS projected were calculated for the both $Al_2(WO_4)_3$ models and the results are illustrated in Fig. 3(a–d).

An analysis of the band structure displayed in Fig. 3(a and b) show that the band gap values are indirect ($\Gamma \rightarrow Z$) and direct ($\Gamma \rightarrow \Gamma$) transitions for s and s^* models, respectively. A noticeable decrease of the band gap energy from going to fundamental s (6.16 eV) to exited s^* (5.84 eV) electronic state is sensed. An analysis of the DOS projected on atoms and orbitals for the s and s^* models presented in Fig. 3(c and d) indicate that uppermost levels in the VB consist mainly of O 2p orbitals with a lower contribution of W 5d and Al 4s orbitals, while the CB is formed mainly by the W 5d and O 2p orbital states with a small contribution of Al 4s orbitals. The distortion process from the fundamental to excited tetrahedral [WO$_4$] clusters provokes the decrease of the band gap value, and we sense a difference between the atomic orbital contributions in s and s^* models, in particular for the W 5d orbitals. Our findings suggest an increase in the contribution of the W atoms related to 5d_{xy} and 5d_{yz} orbitals levels in s^* state compared to the ground state, and thus they have a more important role for the PL behavior of $Al_2(WO_4)_3$ powders.

An analysis of site- and orbital-resolved DOS shows that the W CB DOS depends significantly on the local coordination. During the excitation process some electrons are promoted more feasibly from the O 2p states to the W5d states in (5d_{xy} and 5d_{yz} orbitals) through the absorption of photons. These results show that the properties of this material are strongly influenced by the degree of structural order–disorder, which provides a change in the transition from indirect-to-direct band gap at fundamental s and excited, s^*, electronic states, respectively. The changes result in a decrease of the band gap energy for the $Al_2(WO_4)_3$ powders.

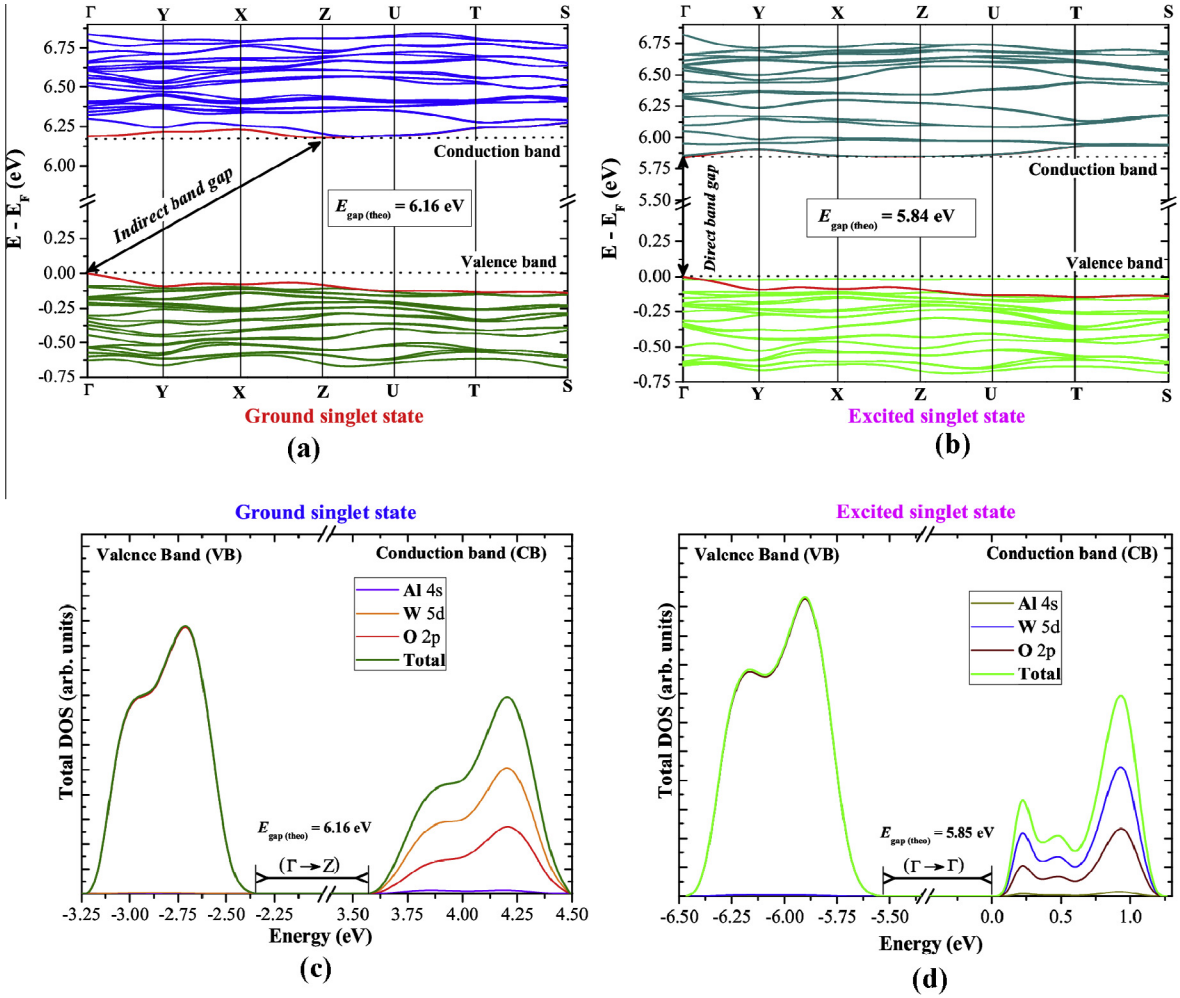

Fig. 3. (a and b) Band structures and (c and d) projected DOS on atomic levels for both o-$Al_2(WO_4)_3$ and d-$Al_2(WO_4)_3$ models.

Based on this theoretical information for the *s* model, E_{gap} values of $Al_2(WO_4)_3$ powders were calculated using $n = 0.5$. Finally, using the remission function described in Eq. (3) with $k = 2\alpha$, we obtain the modified Kubelka–Munk equation as indicated in Eq. (4):

$$[F(R_\infty)h\nu]^2 = C_2(h\nu - E_{gap}) \quad (4)$$

Therefore, finding the $F(R_\infty)$ value from Eq. (4) and plotting a graph of $[F(R_\infty)h\nu]^2$ against $h\nu$, we can determine the E_{gap} values for our $Al_2(WO_4)_3$ powders with greater accuracy by extrapolating the linear portion of the UV–vis curves. In general, different types of defects generated during the synthesis enable a change in its optical transitions offering an opportunity to tune their properties by the band gap engineering.

Fig. 4(a–e) shows UV–vis spectra for $Al_2(WO_4)_3$ powders heat-treated at 100, 200, 400 °C, 800 °C and 1000 °C for 2 h.

Evidently, powders have different E_{gap} values which are possibly related to the existence of new energy levels near the CB, which were confirmed by theoretical calculations. The E_{gap} value is low (from 3.16 to 3.48 eV) for $Al_2(WO_4)_3$ powders heat-treated at 100 °C, 200 °C and 400 °C for 2 h (see Fig. 4(a–c)) which indicates a high defect concentration and intermediate levels between the VB and CB for these powders. However, for $Al_2(WO_4)_3$ powders heat-treated at 800 °C and 1000 °C for 2 h, we observed typical absorption spectra for crystalline materials or an ordered structure (see Fig. 4(d and e)).

We analyzed the charge density contour for the single (*s*) and excited single (*s**) models, as illustrated in Fig. 5(a and b). These electronic density maps were generated to provide in-depth insight into the molecular geometry, symmetry breaking and electronic order–disorder effects for these models.

Our theoretical results reveal a possible hybridization between 5d (W) and 2p (O) linked to (W–O) bond presents in tetrahedral $[WO_4]$ clusters. A displacement of W atoms from the ideal center in tetrahedral $[WO_4]$ clusters was performed to represent the *s* model. These electronic perturbations promote an increase in the charge density on the atomic sites forming the trigonal pyramidal $[WO_3]$ clusters, which are assigned *s** model, as can be viewed in Fig. 5(a and b)). These theoretical calculated results indicate the possible effects on their structure and electronic properties that involves the presence of the *s** in disordered lattice, which could be the main responsible of PL behavior in disordered $Al_2(WO_4)_3$ powders.

PL emission analyses of $Al_2(WO_4)_3$ powders

Fig. 6(a–e) illustrate the PL emission spectra at room temperature of $Al_2(WO_4)_3$ powders obtained by coprecipitation and heat-treated at different temperatures for 2 h.

Blasse and Ouwerkerk [18] have been proposed that PL properties of $Al_2(WO_4)_3$ crystals are related to self-localized excitons and electronic transitions within the two types of tetrahedral $[WO_4]$

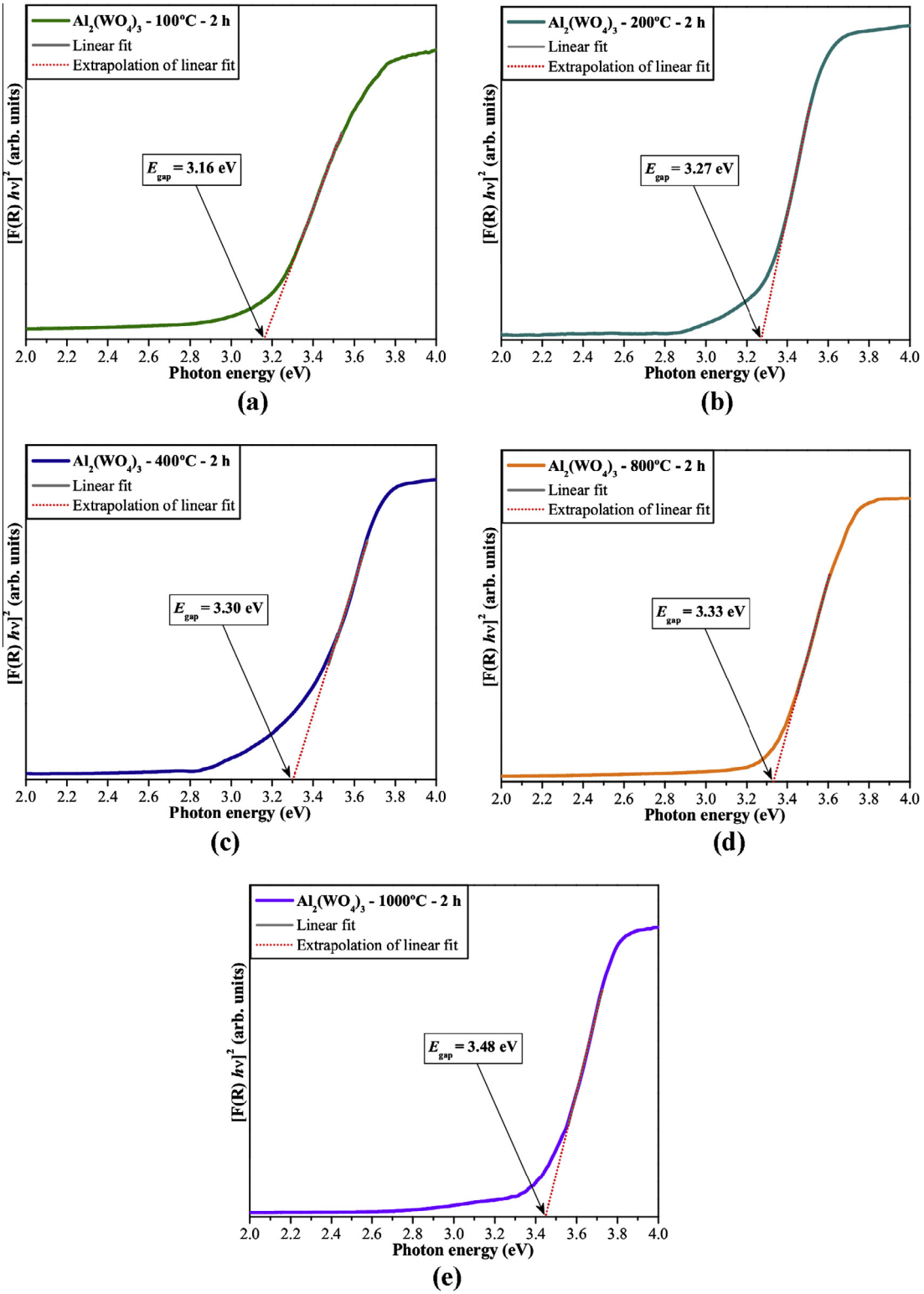

Fig. 4. UV–vis spectra for the $Al_2(WO_4)_3$ powders heat-treated at: (a) 100 °C, (b) 200 °C, (c) 400 °C, (d) 800 °C and (e) 1000 °C for 2 h, respectively.

clusters in their crystal structure, while Kotlov et al. [55] suggested that free electrons and holes are created in this material due to electronic transitions from oxygen to cation states which are situated several electron volts above the bottom of the CB. In this research, we have observed a highly intense PL emission at room temperature. Based on our structural and electronic investigations, we ascribe this PL behavior to structural and electronic order–disorder effects of tetrahedral $[WO_4]$ clusters in $Al_2(WO_4)_3$ powders. Our theoretical results suggest that structural and electronic order–disorder effects cause a polarization of one type of tetrahedral $[WO_4]$ clusters that facilitates the population of electronic excited states, and they may return to lower energy and fundamental states via radiative and/or non-radiative relaxations, which promotes a intense PL emission in $Al_2(WO_4)_3$ powders.

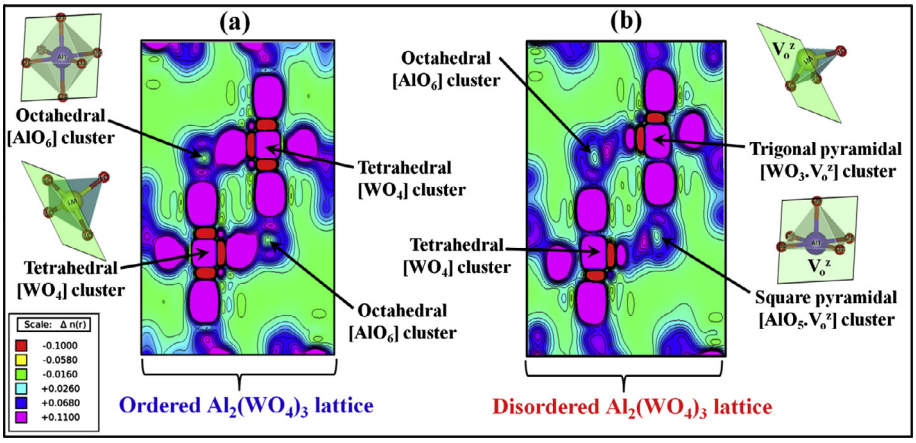

Fig. 5. Charge density maps in (a) ordered and (b) disordered $Al_2(WO_4)_3$ models.

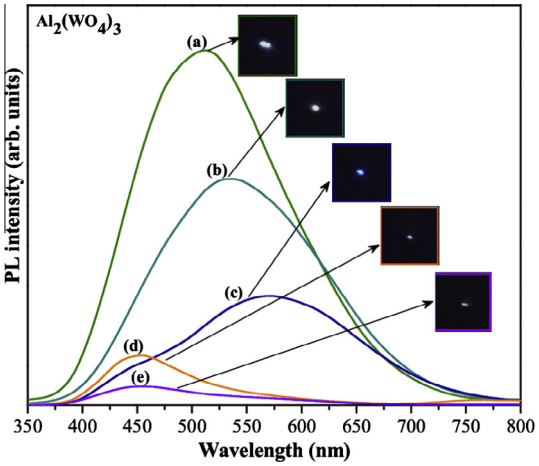

Fig. 6. PL emission spectra for the $Al_2(WO_4)_3$ powders heat-treated at (a) 100 °C, (b) 200 °C, (c) 400 °C, (d) 800 °C and (e) 1000 °C for 2 h, respectively.

Conclusions

In summary, $Al_2(WO_4)_3$ powders were synthesized by the CP method at room temperature without surfactants and heat-treated at different temperatures for 2 h. XRD patterns indicate that crystalline $Al_2(WO_4)_3$ powders obtained by the CP method and heat-treated at 800 °C and 1000 °C have an orthorhombic structure with a space group *Pnca*. FE-SEM images revealed large particles for crystalline $Al_2(WO_4)_3$ powders with irregular shapes. Particle growth is related to mass transport mechanisms via nanocrystalline particle diffusion during the sintering process by an increase of the heat treatment. UV–vis spectra show an increase in the optical band gap with a calcination temperature which raise and suggest a direct allowed transition with the existence of intermediary energy levels between the VB and CB. Stable electronic excited states (singlet) have been characterized by using DFT method at the B3LYP calculation level of model. The analysis of the band structures and density of states of both ground and first excited electronic states allows a deep insight on the main electronic features based on structural and electronic order–disorder effects of both octahedral [AlO_6] and tetrahedral [WO_4] clusters, as constituent building units of this material. These findings confirm that PL is directly associated with structural and electronic order–disorder effects in one type of tetrahedral [WO_4] cluster, which facilitates the population of electronic excited states and furthers our understanding of the behavior of PL in these materials. Our results offer new ideas and perspectives with regard to the behavior of optical materials and suggest that these materials are promising for applications in photovoltaic devices and catalysis.

Acknowledgments

The Brazilian authors acknowledge the financial support of the Brazilian research financing institutions: CNPq (304531/2013-8), FAPESP (09/50303-4; 12/18597-0), and CAPES. The Spanish authors would like to thank the Spanish Government MAT2010-21088-C03 project and the Catalan Government PIGC project 2009-SGR-0674. J. Andrés acknowledges Generalitat Valenciana (Prometeo/2009/053 project), Ministerio de Ciencia e Innovación (CTQ-2012-36253-C03-01) Programa de Cooperación Científica con Iberoamerica (Brazil), Ministerio de Educación (PHB2009-0065-PC project).

Appendix A. Supplementary material

Supplementary data associated with this article can be found, in the online version, at http://dx.doi.org/10.1016/j.molstruc.2014.10.016.

References

[1] G.D. Mukherjee, S.N. Achary, A.K. Tyagi, S.N. Vaidya, J. Phys. Chem. Solids 64 (2003) 611–614.
[2] N. Garg, V. Panchal, A.K. Tyagi, S.M. Sharma, J. Solid State Chem. 178 (2005) 998–1002.
[3] V. Sivasubramanian, T.R. Ravindran, S. Kalavathi, A.K. Arora, J. Electroceram. 17 (2006) 57–60.
[4] M. Maczka, V. Nikolov, K. Hermanowicz, A. Yordanova, M. Kurnatowska, J. Hanuza, Opt. Mater. 34 (2012) 1048–1053.
[5] J.J. de Boer, Acta Cryst. B 30 (1974) 1878–1880.
[6] J. Hanuza, M. Maczka, K. Hermanowicz, M. Andruszkiewicz, A. Pietraszko, W. Strek, P. Dereń, J. Solid State Chem. 105 (1993) 49–69.
[7] K. Nassau, H.J. Levinstein, G.M. Loiacono, J. Phys. Chem. Solids 26 (1965) 1805–1816.
[8] I. Koseva, A. Yordanova, P. Tzvetkov, V. Nikoloa, D. Nihtianova, Mater. Chem. Phys. 132 (2012) 808–814.
[9] D. Nihtianova, N. Velichkova, R. Nikolova, I. Koseva, A. Yordanova, V. Nikolov, Mater. Res. Bull. 46 (2011) 2125–2130.
[10] D.C. Craig, N.C. Stephenson, Acta Crystallogr. B 24 (1968) 1250–1255.
[11] K. Nassau, H.J. Levinstein, G.M. Loiacono, J. Phys. Chem. Solids 26 (1965) 1805–1816.
[12] A. Yordanova, I. Koseva, N. Velichkova, D. Kovacheva, D. Rabadjieva, V. Nikolov, Mater. Res. Bull. 47 (2012) 1544–1549.
[13] E. Zhecheva, R. Stoyanova, S. Ivanova, V. Nikolov, Solid State Sci. 12 (2010) 2010–2014.
[14] V. Nikolov, I. Koseva, R. Stoyanova, E. Zhecheva, J. Alloys Compd. 505 (2010) 443–449.
[15] I.I. Koseva, V.S. Nikolov, Bulg. Chem. Commun. 42 (2010) 300–304.
[16] E. Gallucci, S. Ermeneux, C. Goutaudier, M.Th. Cohen-Adad, G. Boulon, Opt. Mater. 16 (2004) 193–197.

[17] N. Imanaka, S. Tamura, M. Hiraiwa, G. Adachi, Chem. Mater. 10 (1998) 2542–2545.
[18] G. Blasse, M. Ouwerkerk, J. Electrochem. Soc. 127 (1980) 429–434.
[19] I. Nikolov, X. Mateos, F. Guell, J. Massons, V. Nikolov, P. Peshev, F. Díaz, Opt. Mater. 25 (2004) 53–58.
[20] G.D. Mukherjee, V. Vijaykumar, S.N. Achary, A.K. Tyagi, B.K. Godwal1, J. Phys.: Condens. Matter 16 (2004) 7321–7330.
[21] D. Nihtianova, N. Velichkova, R. Nikolova, I. Koseva, A. Yordanova, V. Nikolov, Mater. Res. Bull. 46 (2011) 2125–2130.
[22] J.S.O. Evans, T.A. Mary, A.W. Sleight, J. Solid State Chem. 133 (1997) 580–583.
[23] T.A. Mary, A.W. Sleight, J. Mater. Res. 14 (1999) 912–915.
[24] T. Sugimoto, Y. Aoki, E. Niwa, T. Hashimoto, Y. Morito, J. Ceram. Soc. Jpn. 115 (2007) 176–181.
[25] C. Lind, Materials 5 (2012) 1125–1154.
[26] R.J. Speedy, J. Phys.: Condens. Matter 8 (1996) 10907–10918.
[27] T.A. Mulinari, F.A. La Porta, J. Andrés, M. Cilense, J.A. Varela, E. Longo, CrystEngComm 15 (2013) 7443–7449.
[28] L.S. Cavalcante, F.M.C. Batista, M.A.P. Almeida, A.C. Rabelo, I.C. Nogueira, N.C. Batista, J.A. Varela, M.R.M.C. Santos, E. Longo, M. Siu Li, RSC Adv. 2 (2012) 6438–6454.
[29] F.A. La Porta, M.M. Ferrer, Y.V.B. Santana, C.W. Raubach, V.M. Longo, J.R. Sambrano, E. Longo, J. Andrés, M.S. Li, J.A. Varela, J. Alloys Compd. 555 (2013) 153–159.
[30] A.D. Becke, J. Chem. Phys. 98 (1993) 5648–5653.
[31] C. Lee, W. Yang, R.G. Parr, Phys. Rev. B 37 (1988) 785–789.
[32] R. Dovesi, V.R. Saunders, C. Roetti, R. Orlando, C.M. Zicovich-Wilson, F. Pascale, B. Civalleri, K. Doll, N.M. Harrison, I.J. Bush, P.D. Arco, M. Llunell, CRYSTAL09 Users Manual, University of Torino, 2009.
[33] P.J. Hay, W.R. Wadt, J. Chem. Phys. 82 (1985) 299–310.
[34] Available at: http://www.crystal.unito.it/Basis_Sets/Ptable.html.
[35] H.J. Monkhorst, J.D. Pack, Phys. Rev. 13 (1976) 5188–5192.
[36] I. Gadaczek, K.J. Hintze, T. Bredow, Phys. Chem. Chem. Phys. 14 (2012) 741–750.
[37] L. Gracia, J. Andres, V.M. Longo, J.A. Varela, E. Longo, Chem. Phys. Lett. 493 (2010) 141–146.
[38] M.L. Moreira, J. Andres, L. Gracia, A. Beltrán, L.A. Montoro, J.A. Varela, E. Longo, J. Appl. Phys. 114 (2013) 043714–043722.
[39] L. Gracia, V.M. Longo, L.S. Cavalcante, A. Beltran, W. Avansi, M.S. Li, V.R. Mastelaro, J.A. Varela, E. Longo, J. Andres, J. Appl. Phys. 110 (2011) 043501–043511.
[40] M.R.D. Bomio, R.L. Tranquilin, F.V. Motta, C.A. Paskocimas, R.M. Nascimento, L. Gracia, J. Andres, E. Longo, J. Phys. Chem. C 117 (2013) 21382–21395.
[41] A. Kokalj, J. Mol. Graph. Modell. 17 (1999) 176–179.
[42] D.A. Woodcock, P. Lightfoot, C. Ritter, J. Solid State Chem. 149 (2000) 92–98.
[43] H.M. Rietveld, J. Appl. Cryst. 2 (1969) 65–71.
[44] M. Bortolotti, L. Lutterotti, I. Lonardelli, J. Appl. Cryst. 42 (2009) 538–539.
[45] K. Momma, F. Izumi, J. Appl. Crystallogr. 44 (2011) 1272–1276.
[46] J.S.O. Evans, T.A. Mary, A.W. Sleight, J. Solid State Chem. 137 (1998) 148–160.
[47] W. Paraguassu, M. Maczka, A.G. Souza Filho, P.T.C. Freire, F.E.A. Melo, J. Mendes Filho, J. Hanuza, Vib. Spectrosc. 44 (2007) 69–77.
[48] P. Kubelka, F. Munk-Aussig, Zeit. Für. Tech. Physik. 12 (1931) 593–601.
[49] A.E. Morales, E.S. Mora, U. Pal, Rev. Mex. Fis. S 53 (2007) 18–22.
[50] R.A. Smith, Semiconductors, second ed., Cambridge University Press, London, 1978. p. 434.
[51] R. Lacomba-Perales, J. Ruiz-Fuertes, D. Errandonea, D. Martínez-García, A. Segura, Eur. Phys. Lett. 83 (2008) 37002–37006.
[52] L.S. Cavalcante, M.A.P. Almeida, W. Avansi, R.L. Tranquilin, E. Longo, N.C. Batista, V.R. Mastelaro, M. Siu Li, Inorg. Chem. 51 (2012) 10675–10687.
[53] L.S. Cavalcante, V.M. Longo, J.C. Sczancoski, M.A.P. Almeida, A.A. Batista, J.A. Varela, M.O. Orlandi, E. Longo, M. Siu Li, CrystEngComm 14 (2012) 853–868.
[54] E.I. Ross-Medgaarden, I.E. Wachs, J. Phys. Chem. C 111 (2007) 15089–15099.
[55] A. Kotlov, S. Dolgov, E. Feldbach, L. Jönsson, M. Kirm, A. Lushchik, V. Nagirnyi, G. Svensson, B.I. Zadneprovski, Phys. Status Solidi C 2 (2005) 61–64.